Accepted Manuscript

A Simple Synthesis of Nitrogen doped Porous Graphitic Carbon: Electrochemical Determination of Paracetamol in Presence of Ascorbic acid and *p*-Aminophenol

Sudip Biswas, Dipanjan Chakraborty, Rashmita Das, Rajib Bandyopadhyay, Panchanan Pramanik

PII: S0003-2670(15)00905-8

DOI: 10.1016/j.aca.2015.07.045

Reference: ACA 234069

To appear in: *Analytica Chimica Acta*

Received Date: 14 May 2015

Revised Date: 7 July 2015

Accepted Date: 17 July 2015

Please cite this article as: S. Biswas, D. Chakraborty, R. Das, R. Bandyopadhyay, P. Pramanik, A Simple Synthesis of Nitrogen doped Porous Graphitic Carbon: Electrochemical Determination of Paracetamol in Presence of Ascorbic acid and *p*-Aminophenol, *Analytica Chimica Acta* (2015), doi: 10.1016/j.aca.2015.07.045.

A Simple Synthesis of Nitrogen doped Porous Graphitic Carbon: Electrochemical Determination of Paracetamol in Presence of Ascorbic acid and *p*-Aminophenol

Sudip Biswas[1], Dipanjan Chakraborty[1], Rashmita Das[1], Rajib Bandyopadhyay[1], Panchanan Pramanik[2*]

[1]Department of Instrumentation and Electronics Engineering, Jadavpur Universiy Salt lake Campus, Kolkata-700098, India.

[2] Department of Basic Science, MCKV Institute of Engineering, Liluah, West Bengal-711204, India.

E-mail: pramanik1946@gmail.com

ABSTRACT

Graphite paste electrode modified with nitrogen doped porous carbon (NDPC) is used for the detections of paracetamol (PCM), ascorbic acid (AA) and *p*-aminophenol (PAP) at relatively low concentration. NDPC is synthesized by direct carbonization of $Zn(OAc)_2$ incorporated melamine-formaldehyde resin microsphere. The NDPC shows small pore diameters centered at 3.14nm and 8.12nm and has a pseudo graphitic structure with reasonable porous matrix. The limits of detections (S/N=3) for PCM, AA, and PAP are found to be 30nM, 720nM and 10nM respectively. Under optimized experimental condition, the linear ranges of determination for PCM and AA are 1-400µM, 10-2700µM respectively in mixture. Similarly for PCM and PAP mixture, the linear ranges of determination are found to be 1-90µM. It is also used for the analysis of urine and pharmaceutical products with better sensitivity.

Keywords: Nitrogen doped porous carbon, melamine-formaldehyde resin, electrochemical determination, *p*-Aminophenol, Paracetamol

1. Introduction

Paracetamol (PCM) is a well-known antipyretic, non-steroidal and anti-inflammatory drug. It is used mostly for pains associated with backache, headache, cancer, arthritis, postoperative condition and also with viral and bacterial fever [1-3]. Recent studies reveal that it is a preventive for hardening of artery in cardiovascular disease [4]. Recommended doses of PCM do not have any side effect, but overdoses could bring adverse side effects like hepatoxicity and nephrotoxicity [5, 6], it also causes liver disorders, skin rashes and inflammation in pancreas [7]. PCM is easily excreted in urine after oral administration due to its rapid absorption and distribution. So for monitoring PCM concentration in biological fluid, the analysis of urine sample is convenient. The hydrolytic product of PCM is *p*-aminophenol (PAP) which has adverse side effects on kidneys and physiological growth of the body. The lower limit of body tolerance of PAP is 50 ppm [8]. So monitoring of PAP in the presence of PCM in biological fluid is desirable after administration. Therefore, development of fast, simple and accurate analytical technique for the determinations of PCM and its hydrolyzed product is of great importance. Ascorbic acid (AA) is a natural antioxidant and an important vitamin in living system [9]. AA has an important role in collagen formation and helps in iron uptake through reduction [10]. It is used as an auxiliary medicine for common cold, mental illness, infertility, cancer and AIDS [11]. The metabolic product of AA is oxalic acid, which causes the renal problem. Deficiency of AA leads to anemia, deterioration of collagen, skin hemorrhages, lowering the body resistance from infections [12]. It also causes thyroid deficiency and premature aging [13]. On the other hand, high level of AA causes gastric irritation and diarrhea [14]. Also AA is an interfering biomolecule during PCM analysis in body fluid. Thus, analyses of mixtures of PCM with PAP and PCM with AA are of great importance. Several analytical techniques for above mentioned analysis have been developed using liquid

chromatography [15], spectrophotometry [16], chemiluminasence, flow injection methods [17], capillary electrophoresis [18], colorimetry [19], FTIR-Raman spectrometry [20]. But these methods are often expensive and time consuming with low sensitivity and selectivity. As PCM, PAP and AA are electro-active compounds; therefore electrochemical technique for the determination of PCM drew a lot of attention in the last few years due to its simplicity, low cost, high sensitivity and selectivity.

Carbon materials with porous morphology, small pore diameter and large surface area have taken lots of attention for better electrocatalytic properties [21-24]. In this regard, electrode materials made up of carbon nanotube film modified glassy carbon electrode [25-31], graphene modified glassy carbon electrode [32], Nafion/TiO_2-graphene modified electrode [33], C_{60}-modified glassy carbon electrode [34], polyaniline-multi wall carbon nanotube electrode [35], carbon film resistor electrode [36], hematoxiline biosensor [37], polyphenol oxidase modified glassy carbon electrode [38], multiwalled carbon nanotube/pyrolytic graphite electrode [39] and boron doped diamond thin film electrode [40] have been developed.

In this present study, a paste of simple composite of nitrogen doped porous carbon (NDPC) with graphite is used as electrode which shows better sensitivity than all the above mentioned methods. We have synthesized porous nitrogen doped carbon by carbonizing $Zn(OAc)_2$ incorporated melamine formaldehyde resin (ZAIMFR) microsphere. Here $Zn(OAc)_2$ is used as an activator. Comparative study of electrocatalytic properties of nitrogen doped porous carbon-graphite paste (NDPC/GP), bare NDPC, bare graphite paste (GP) electrode against PCM, AA and PAP are investigated. Selective determination of PCM in the presence of AA and PAP is done by using differential pulse voltammetry technique. It is observed that the composite of the NDPC/GP electrode shows better analytical performance amongst all the developed electrodes.

2. EXPERIMENTAL

2.1 Chemicals and reagents

Formaldehyde, Zinc Acetate dihydrate, Ascorbic acid, *p*-aminophenol, Paracetamol, Sodium dihydrogen phosphate, Sodium hydroxide, and Paraffin oil were obtained from Merck, India and Graphite flakes, Melamine were purchased from Sigma Aldrich, USA. All the reagents were analytical graded and used without further purification. All required solutions were prepared using Millipore water (Resistance 18MΩ).

2.2 Apparatus and measurements

The morphology of synthesized NDPC was determined by JEM2100 high resolution transmission electron microscope (HRTEM) and JEOL JEM6700F field emission scanning electron microscopy (FESEM). The TEM sample was prepared by drying a droplet of suspended NDPC on a carbon coated Cu grid. Nitrogen adsorption-desorption isotherms and Brunauer-Emmett-Teller (BET) surface areas were measured by using Beckmam Coulter SA3100 at 77K. The sample was degassed at 130^0C for 3hrs. Powder X-ray diffraction (PXRD) was carried out with an X-ray diffractometer (XRD, D/MAX-RA, Japan) operated at 40KV and 40mA with $Cu_{K\alpha}$ radiation (λ = 0.15406nm). Fourier transform infrared (FTIR) spectra (KBr dispersed pellets) in the range of 400–4000 cm^{-1} (model Paragon-500 FTIR of Perkin Elmer spectrometer) and Raman spectroscopy were performed with a micro-Raman system (Renishaw, RM1000-In Via) at 514nm. The nitrogen content in NDPC was determined using an elemental analyzer (Vario EL III, Germany). All electrochemical measurements were performed by three electrode system using Autolab Potentiostate/Galvanostate101 (Netherlands). An Ag/AgCl electrode was used as a reference

electrode and Pt electrode as a counter electrode. All the electrochemical studies were carried out in 0.1 (M) phosphate buffer of pH 6 at temperature 25 ± 2^0 C.

2.3 Synthesis of nitrogen doped porous carbon

Formaldehyde (9.8g, 37%) was added to 200ml of millipore water in a beaker and heated up to 80^0C and subsequently 2.5g of melamine was added to it and stirred till to get a clear solution. 1.5g $Zn(OAc)_2$, $2H_2O$ was added to the above clear solution with continuous stirring and immediately the solution turned turbid, which disappeared with the addition of a few drops of acetic acid. After that, the solution was kept in a hot air oven for 12hrs at 120^0C to produce a white powdery mass.

To obtain NDPC, the white mass was carbonized in horizontal tube furnace at 950^0C for 1hr with a heating rate of 7^0C/min under the continuous flow of N_2 gas. The obtained black powder was collected and complete removal of Zn species was confirmed by Energy dispersive X-ray spectroscopy (EDS) (Figure 2d).

2.4 Preparation of the NDPC/GP electrode

Graphite flakes and prepared NDPC were mixed in 1:1(w/w) ratio in a mortar and paraffin oil was added, followed by grinding for making a paste. Finally, the paste was put into a capillary glass tube of 2mm inner diameter and packed tightly by pressing with a metal rod. Electrical connection was taken by putting a Cu-wire from the backside of the glass tube. Bare graphite and NDPC paste electrodes were prepared in the similar method. Before experimentation, electrode surface was cleaned with 0.3µm and 0.05µm Al_2O_3 slurries, rinsed with ethanol and dried under N_2.

3. RESULTS AND DISCUSSIONS

3.1 Formation mechanism of NDPC

Scheme 1

Scheme 1 is showing a graphical representation of the formation of NDPC, which is synthesized through four major steps. In the 1st step melamine is reacted with formaldehyde to form a clear aqueous solution of melamine-formaldehyde resin (MFR) at 80^0C. In the 2nd step, $Zn(OAc)_2$ $2H_2O$ is added to the solution and dissolved, after that the solution has been kept at 120^0C for 12hrs for extended polymerization. During this period cross-linking among MFR takes place and eventually zinc acetate incorporated MFR (ZAIMFR) microsphere is formed in the 3rd step. In the last step, during thermal annealing at 950^0C, all the Zn species are reduced to metallic zinc (*b.p* 904^0C) and evaporated out from the sample to make a porous N-doped carbon [41]. The nitrogen content in the NDPC is measured by EDS as 12.6 atomic wt. percentages (Figure 2d) and also by elemental analysis which shows 12.2 atomic wt. percentages.

3.2 XRD analysis of prepared NDPC

Figure 1

The wide angle X-ray diffraction (XRD) patterns of synthesized ZAIMFR and NDPC are shown in Figure 1a, b. It is noted that the XRD of spherical ZAIMFR (Figure 1a) shows the presence of $Zn(OAc)_2$, $2H_2O$ with a little amount of ZnO. The XRD of NDPC (Figure 1b) consists of two well defined broad graphitic peaks at $2\theta = 24.8^0$ and 43.2^0 corresponding to the carbon (002) and (101) crystal plane diffraction, respectively. The later one arises due to graphitic stacking [42]. The inter planner spacing (d_{002}) is 0.358nm which is pretty close to the single crystal graphite (0.335nm). It implies that NDPC has graphite like structure. The weak diffraction peak (002) plane is indicating

low degree of graphitization with parallel single layers [43]. During carbonization when temperature is higher than 800^0C, Zn ions are reduced to metallic zinc and ultimately evaporated out at the elevated temperature (*b.p* 906^0C) which is confirmed by x-ray diffraction (XRD) and electron dispersive spectroscopy (EDS) of NDPC [44] (See Supplementary Information, Table S1).

3.3 FESEM and TEM of NDPC

Figure 2

The morphological studies of the prepared ZAIMFR and NDPC are carried out by transmission electron microscopy (TEM) and field emission scanning electron microscopy (FESEM) and presented in Figure 2a, b, c (See Supplementary Information, Figure S1 and S2). The FESEM (Figure 2a) of prepared ZAIMFR has the same spherical morphology as reported previously with a diameter ranging around 1 to 3 micrometers [45]. From the TEM image of NDPC, we can see clearly the random orientation of multi layer graphic domains. This is in agreement with the above mention XRD results. During pyrolysis at above 906^0C temperature all Zn metals are evaporated out and results a porous structure with irregular morphology of NDPC (Figure 2d, c).

3.3 FTIR and Raman Study

Figure 3

Fourier transform infrared (FTIR) spectroscopy is done to infer the degree of carbonization of NDPC. Figure 3a shows the FTIR transmittance spectra of ZAIMFR (red) and NDPC (black). The reaction between melamine with formaldehyde proceeds through hydroxymethylation where the

H-atoms of NH_2 groups of melamine are substituted by methylol ($-CH_2OH$) groups followed by cross linking of the methylolamines. The stretching of O-H in MFR overlaps with the bending vibration of NH_2, resulting a broad peak at 3105-3455cm^{-1}. The two weak peaks at 2866 and 2940cm^{-1} indicate stretching bands of C-H. The peak at 1330cm^{-1} is related to the C-N stretching of the secondary/tertiary amine group. The FTIR Peaks at 814, 1002 and 1150cm^{-1} correspond to C-N-C, ether(C-O-C) and amino group respectively. The triazine unit in MFR shows two peaks at 1570 and 1470cm^{-1}. A broad peak at 430-680cm^{-1} is consistent with Zn-O. During pyrolysis of MFR, rupture of triazine units takes place between 600^0C to 675^0C [46] and above 906^0C all metallic Zn evaporate out. The mutual effects of these two lead to the formation of porous NDPC.

Raman spectrum of NDPC is showing two well distinct peaks within a range of 1360-1600cm^{-1} due to the presence of aromatic ring structure and crystalline nature. Two peaks, one at 1362cm^{-1} and another at 1581cm^{-1} are corresponding to disordered D and G bands respectively, indicating the formation of graphitic structure [44]. A low intense broad peak at 2931cm^{-1} arises for a large amount of N doping. The lower value of the I_G/I_D (≈0.77) is an indication of better extent of graphitic ordering. This is in agreement with the XRD and TEM results.

3.4 BET N_2 adsorption-desorption analysis

Figure 4

BET N_2 adsorption-desorption isotherm at 77K and corresponding Barrett-Joyner-Halenda (BJH) pore size distribution curve of NDPC are shown in Figure 4a, b. N_2 adsorption-desorption isotherms (Figure 4a) shows a type VI curve with the corresponding BET surface area of 7m^2/g. However BJB pore diameter distribution (Figure 4b) shows that the obtained NDPC is mesoporous

in nature with an average pore diameter distribution of 3.14 and 8.12nm respectively. The pore diameters (larger than 2nm) are suitable for faster mass transfer of molecules and ion diffusion in aqueous electrolyte. Owing to narrow pore diameter of 3.14 and 8.12nm and relatively large surface area of NDPC are expected to have good electrocatalytic material.

3.5 Electrochemical properties study of NDPC/GP, bare GP and NDPC electrodes

Figure 5

A comparative electrocatalytic properties of the electrodes have been studied using $[Fe(CN)_6]^{-3}/[Fe(CN)_6]^{-4}$ system as a reference. The cyclic voltammograms obtained for 1mM $K_4[Fe(CN)_6]$ solution using bare GP, bare NDPC and NDPC/GP electrodes are presented in Figure 5a. The peak potential separation (ΔE_p) at NDPC/GP electrode is 97mV and that for bare GP and bare NDPC electrodes are 259mV and 185mV respectively. It is observed that the electron transfer rate increases with a decrease in the value of ΔE_p [47]. This means that the electron transfer rates are in the order of NDPC/GP>bare NDPC>bare GP electrode. The redox peak current is highest for the NDPC/GP electrode; this may arise due to low pore diameter and good electrical conductivity. All these results show that NDPC/GP is significantly better than bare GP or NDPC electrode. NDPC/GP shows maximum peak current at pH 6 (Figure 5b), so all the experimental works have been carried out at this optimum pH.

3.6 Electrocatalytic oxidation of PCM, AA and PAP

Figure 6

Electrocatalytic behaviors of each of PCM, AA and PAP at bare GP, NDPC and NDPC/GP have been investigated by cyclic voltammetry (CV) and are presented in Figure 6a, b, c. CVs of PCM (Figure 6a) show a quasi-reversible redox property with redox peak separation (ΔE_p) of 256mV

and 329mV for bare GP and bare NDPC electrodes respectively, however, in case of NDPC/GP it becomes only 188mV with significant increase in peak current. This indicates better reversibility and electrocatalytic property of NDPC/GP electrode due to its low pore diameter with large surface area, and also nitrogen doping in the matrix through generation of more active sites. Moreover the NDPC/GP shows nearly two times higher peak current (I_{PCM}) compared to bare GP and NDPC. The peak currents for PCM with different scan rates ranging from 5 to 400mVs^{-1} have been shown in supplementary information, Figure S3. It is observed that peak current increases linearly with increasing scan rate which indicates that, it is a surface controlled process. The oxidation behavior of AA at different electrodes is given in Figure 6b. AA shows the irreversible oxidation character at all three electrodes. There is a negative shift of the oxidation peak potential of 68mV and 27mV at NDPC/GP (271mV) compared to bare GP (339mV) and NDPC (298mV) electrode respectively. It is clearly observed that the CV oxidation peak current (I_{AA}) of AA for NDPC/GP, GP and NDPC electrodes are 10.55µA, 3.4µA and 9.53µA respectively. It is also found that the peak current value at NDPC/GP is 3.1 and 1.12 times higher than that of bare GP and NDPC respectively (Figure 6f).

The CV plots of PAP show (Figure 6c) a quasi-reversible redox behavior for all three electrodes. The oxidation peak potential (E_{PAP}) at NDPC/GP is 202mV which shows a positive shift of 12mV and 3mV than that of peak potentials at bare GP (190mV) and NDPC (199mV) respectively (Figure 6c). Differential pulse voltammetry (DPV) over CV is applied, for the simultaneous determination of PCM with AA and PAP, due to its higher sensitivity. Differential pulse voltammetry (DPV) plots of PCM with AA and PAP are shown in Figure 6d, e. DPV of PCM and AA mixture shows two well defined oxidation peaks at 421mV and 157mV respectively with a peak potential separation of 264mV. The oxidation peak potential values of PCM and PAP are

obtained at 424mV and 155mV respectively in the PCM and PAP mixture with peak separation of 271mV.

3.7 Simultaneous determination of PCM and AA

Figure 7

For the simultaneous determination of AA and PCM in the mixture, the measurements are done by varying the concentration of one of the constituents with keeping the other one at constant concentration. Figure 7a illustrates the DPVs of 1mM AA with varying concentrations of PCM at 0.1M phosphate buffer solution of pH 6. The oxidation peak currents (I_{PCM}) of PCM increases linearly with increasing concentration (C_{PCM}) of PCM (Figure 7c) in a range of 1µM to 7µM following the regression equation I_{PCM} (µA) = $4\times10^{-7}C_{PCM} + 3\times10^{-7}$ with R^2=0.99 and again the linear response is obtained from 8µM to 400µM subsequent to regression equation I_{PCM} (µA) = $4\times10^{-8}C_{PCM} + 3\times10^{-6}$ with R^2=0.98. The 1st linear response in the calibration curve arises due to sub mono-layer adsorption and 2nd linear response curve indicates the formation of a monolayer-covered surface [48] at NDPC/GP electrode. Determination of concentration of AA in the presence of PCM is carried out by varying the concentration of AA at a constant concentration of PCM at 0.1mM (Figure 7b). It is observed that the oxidation peak current (I_{AA}) of AA increases linearly with concentration (C_{AA}) (Figure 7d) from 10µM to 2700µM with the analogous regression equation $I_{AA}=7\times10^{-9}C_{AA}+2\times10^{-7}$ and R^2=0.99.

3.8 Simultaneous determination of PAP and PCM

Figure 8

Simultaneous determinations of PAP and PCM in a mixture are done by varying the concentration of two constituents in equal gradient (Figure 8a). Linear response curves are obtained for the concentrations of PCM and PAP from 1µM to 90µM with peak current (Figure 8b). For PCM, linear regression equation is $I_{PCM} = 6E^{-08} \times C_{PCM} + 1E^{-07}$ ($R^2 = 0.9921$) and for PAP linear regression is $I_{PAP} = 2 \times E^{-07} C_{PAP} + 5E^{-07}$ ($R^2 = 0.9900$). The detection limits (S/N=3) of PCM, AA and PAP are 30nM, 720nM and 10nM respectively.

3.9 Simultaneous determination of AA, PCM and PAP

Figure 9

Simultaneous determinations of AA, PCM and PAP are presented in Figure 9a, b. Figure 9a is showing variation of the concentration of AA with PCM keeping PAP at a constant concentration of 10µM. AA shows (inset) a linear response from 10µM to 2500µM following the regression equation $I_{AA} = 0.008C_{AA} + 3.69$ (R^2=0.97) and that for PCM is from 1 to 350µM (inset) having the regression equation $I_{PCM} = 0.0533C_{PCM} + 1.2$ (R2=0.98). Figure 9b is showing variation of the concentration of PAP with PCM keeping the concentration of AA constant at 10µM. Here PCM and PAP both show $I_{PCM/PAP}$ *vs.* $C_{PCM/PAP}$ linear response from 1µM to 90 µM (inset). For PCM, the regression equation is $I_{PCM} = 0.0739C_{PCM} - 0.19$ (R^2=0.98) and that for PAP is $I_{PAP} = 0.208C_{PAP} - 0.24$($R^2$=0.98). All these above results indicate that determination of PCM with AA and PAP at NDPC/GP electrode is achieved with good selectivity and sensitivity. A comparison with the previously reported data is summarized in Table 1. It is noticed that the NDPC/GP electrode shows

better or comparable analytical results including detection limit and linear range than the previously reported works. Especially the detection limits for PAP and PCM are significantly low.

Table 1

3.10 Reproducibility and stability

To evaluate the reproducibility of NDPC/GP electrode for PCM, five successive DPV measurements (Supplementary information, Figure S4) are carried out with 0.1mM of PCM, 0.1mM of AA and 0.1mM of PAP in their mixture. The relative standard deviation (R.S.D) of oxidation peak current of PCM is 4.2%. Moreover, the measurements are carried out after 3 weeks at room temperature with NDPC/GP electrode which show no significant decrease in oxidation peak currents in DPV (1.6% for PCM, 3.4% for AA and 1.2% for PAP). These results obtained from NDPC/GP have good reproducibility and stability.

3.11 Interference study

The interferences of different substrates during the determination of PCM with NDPC/GP are investigated under optimum condition (80µM PCM at pH 6). The commonly interfering agents such as glucose, sucrose, citric acid, ethanol, Na^+, K^+, Mg^{2+}, SO_4^{2-}, NH_4^+, Fe^{2+}, Fe^{3+}, CO_3^{2-}, Cl^-, alanine, creatinine, adenine phenylalanine, glycine, folic acid, ascorbic acid, dopamine, uric acid and urea with PCM in pharmaceuticals or biological fluids are mixed with the solution. The results show that there is no significant change of current for the determination of PCM i.e. error is less than ±2µA.

3.12 Real sample analysis

For real sample analysis, we have taken paracetamol (tablet and injection) from the local drug store and urine for biological fluid. Urine sample is collected after 4hrs of taking PCM tablet. The urine sample is diluted with 0.1(M) phosphate buffer (pH 6) to an appropriate level, *i.e*. 40 times to fit the calibration curve. The results obtained for real samples are summarized in supporting information (See in Supplementary Information, Table S2, 3). The recovery values for PCM, AA and PAP in urine sample are 102.0%, 99.90% and 101.2% respectively. PCM injection is diluted 20 times with 0.1(M) phosphate buffer (pH 6) and another solution of PCM is prepared by grinding PCM tablet. The recovery values for PCM in tablet and injection are 100.3%, 100.7% respectively. All these results confirm that the NDPC/GP electrode has great potential for the analysis of PCM with AA and PAP in real samples.

4 Conclusion

In summary, we have successfully synthesized nitrogen doped porous carbon with a narrow pore diameter, porous matrix and high nitrogen content from easily available precursors. Electrochemical sensor based on NDPC/GP has been developed for the determinations of paracetamol with its hydrolytic product toxic *p*-aminophenol and ascorbic acid in the mixture. It gives favorable results for the determination of paracetamol in pharmaceuticals as well as in biological fluids. The described methodology is simple, rapid and provides a potent analytical platform for the detection of paracetamol in clinical practice and for quality control in the pharmaceutical industry.

Acknowledgements

The authors are grateful to Council of Scientific and Industrial Research (CSIR) India for financial support for this work. We are also thankful to the UGC Centre for Research in Nanoscience and Nanotechnology (CRNN), University of Calcutta for their HRTEM and FESEM imaging facilities.

Appendix A. Supplementary data

FESEM, more TEM images of ZAIMFR and NDPC respectively, PCM with different scan rate, reproducibility and real samples analyses.

References

[1] J. Koch-Weser, Drug Therapy: Acetaminophen, New Engl. J. Med. 1976, 295, 1297-1300.

[2] S. P. Clissold, Paracetamol and phenacetin, Drugs.1986, 32, 46-59.

[3] C. J. Nikles, M. Yelland, C.D. Marc, D. Wilkinson, The role of paracetamol in chronic pain: an evidence-based approach, Am. J. Therap. 2005, 12, 80-91.

[4] A. A. Taylor, et al., Baylor College of Medicine-Abstract from Munich Meeting Thirteenth IUPHAR Congress of Pharmacology, 1998.

[5] N. Wangfuengkanagul, O. Chailapakul, Electrochemical analysis of acetaminophen using a boron-doped diamond thin film electrode applied to flow injection system, J. Pharm. Biomed. Anal. 2002, 28, 841-847.

[6] C. Lorz, P. Justo, A. Sanz, D. Subirá, J. Egido, A. Ortiz, Paracetamol-Induced Renal Tubular Injury: A Role for ER Stress. J. Am. Soc. Nephrol. 2004, 15, 380–389.

[7] P. I. Dargan, A. L. Jones, Acetaminophen poisoning: an update for the intensivist, Critical Care, 2002, 6, No 2.

[8] The European Pharmacopeial Convention, The Sixth Edition European Pharmacopoeia, The European Pharmacopeial Convention, 2007, pp. 4.

[9] M. C. De Tullio, Beyond the antioxidant: the double life of vitamin C, Subcell. Biochem. 2012, 56, 49-65.

[10] L. Hallberg, M. Brune, L. Rossander. The role of vitamin C in iron absorption, Int J. Vitam. Nutr. Res. Suppl. 1989, 30, 103-108.

[11] J. Thomson, M. Manore, L. Vaughan, The Science of Nutrition, 3rd ed., Benjamin Cummings: San Francisco, CA, 2013, Chapter 10.

[12] K. A. Naidu, Vitamin C in human health and disease is still a mystery? Nutrition Journal, 2003, 2, 7.

[13] R. Moncayo, A. Kroiss, M. O. F. Karakolcu, M. Starzinger, K. Kapelari, H. Talasz, H. Moncayo, The role of selenium, vitamin C, and zinc in benign thyroid diseases and of selenium in malignant thyroid diseases: Low selenium levels are found in subacute and silent thyroiditis and in papillary and follicular carcinoma, BMC Endocrine Disorders, 2008, 8, 2.

[14] N. Mikirova, J. Casciari, A. Rogers, Effect of high-dose intravenous vitamin C on inflammation in cancer patients, J. Transl. Med. 2012, 10, 189.

[15] H. Senyuva, T Ozden, Simultaneous high-performance liquid chromatographic determination of paracetamol, phenylephrine HCl, and chlorpheniramine maleate in pharmaceutical dosage forms, J. Chromatogr. Sci. 2002, 40, 97-100.

[16] P. Nagaraja, K. C. Murthy, K. S. Rangappa, Spectrophotometric method for the determination of paracetamol and phenacetin J. Pharm. Biomed. Anal. 1998, 3, 501-506.

[17] W. Ruengsitagoon, S. Liawruangrath, A, Townshend, Flow injection chemiluminescence determination of paracetamol, Talanta, 2006, 69, 976-983.

[18] S. Zhao, W. Bai, H. Yuan, D. Xiao, Detection of paracetamol by capillary electrophoresis with chemiluminescence detection, Anal. Chim. Acta, 2006, 559, 195–199.

[19] F. Shihana, D. Dissanayake, P. Dargan, A. Dawson, A modified low-cost colorimetric method for paracetamol (acetaminophen) measurement in plasma Clinical Toxicology, 2010, 48, 42–46.

[20] N. Al-Zoubi, J. E. Koundourellis, S. Malamataris, FT-IR and Raman spectroscopic methods for identification and quantitation of orthorhombic and monoclinic paracetamol in powder mixes J. Pharm. Biomed. Anal., 2002, 29, 459-467.

[21] Nada, G. Ahmed, R. A. Ahmed, Simultaneous Determination of Catecholamines and Serotonin on Poly(3,4-ethylene dioxythiophene) Modified Pt-Electrode in Presence of Sodium Dodecyl Sulfate, J. Electrochem. Soc. 2011, 158, F52-F60.

[22] P. Gai, H. Zhang, Y. Zhang, W. Liu, G. Zhu, X. Zhang, J. Chen, Electrochemical determination of acetaminophen using a glassy carbon electrode coated with a single-wall carbon nanotube-dicetyl phosphate film, J. Mater. Chem. B, 2013, 1, 2742-2749.

[23] X. Lijian, D. Jingjing, D. Yan, H. Nongyue, Electrochemical Detection of E. coli O157:H7 Using Porous Pseudo-Carbon Paste Electrode Modified with Carboxylic Multi-Walled Carbon Nanotubes, Glutaraldehyde and 3-Aminopropyltriethoxysilane. J. Biomed. Nanotechnol. 2012, 8, 1006-1011.

[24] S. Biswas, R. Das, D. Chakraborty, R. Bandhyopadhyay, P. Pramanik, Synthesis of Nitrogen Doped Multilayered Graphene Flakes: Selective Non-enzymatic Electrochemical Determination of Dopamine and Uric Acid in presence of Ascorbic Acid. Electroanalysis, 2015, 27, 1253–1261.

[25] D. Sun, H. Zhang, Electrochemical determination of acetaminophen using a glassy carbon electrode coated with a single-wall carbon nanotube-dicetyl phosphate film Microchimica Acta, 2007, 158, 131-136.

[26] B. Habibia, M. Jahanbakhshia, Md. H. Pournaghi-Azarb, Simultaneous determination of acetaminophen and dopamine using SWCNT modified carbon–ceramic electrode by differential pulse voltammetry, Electrochimica Acta, 2011, 56, 2888–2894.

[27] A. A. Ensafi, H. Karimi-Maleh, S. Mallakpour, M. Hatami, Simultaneous determination of N-acetylcysteine and acetaminophen by voltammetric method using N-(3,4-dihydroxyphenethyl)-3,5-dinitrobenzamide modified multiwall carbon nanotubes paste electrode, Sensors and Actuators B: Chemical, 2011, 155, 464–472.

[28] M. Arvand, T. M. Gholizadeh, Simultaneous voltammetric determination of tyrosine and paracetamol using a carbon nanotube-graphene nanosheet nanocomposite modified electrode in human blood serum and pharmaceuticals, Colloids and Surfaces B: Biointerfaces, 2013, 103, 84– 93.

[29] N. Nasirizadeh, Z. Shekari, H. R. Zare, A. Y. Seied, A. Ahmare, Hamid Ahmare, Developing a Sensor for the Simultaneous Determination of Dopamine, Acetaminophen and Tryptophan in Pharmaceutical Samples Using a Multi-Walled Carbon Nanotube and Oxadiazole Modified Glassy Carbon Electrode, J. Braz. Chem. Soc., 2013, 24,1846-1856.

[30] A. B. Moghaddam, A. Mohammadi, S. Mohammadi, D. Rayeji, R. Dinarvand, M. Baghi, R. B. Walker, The determination of acetaminophen using a carbon nanotube:graphite-based electrode, Microchimica Acta, 2010, 171, 377–384.

[31] B. Habibi, M. Jahanbakhshi, M. H. Pournaghiazar, Electrochemical oxidation and nanomolar detection of acetaminophen at a carbon-ceramic electrode modified by carbon nanotubes: a comparison between multi walled and single walled carbon nanotubes, Microchimica Acta, 2011, 172, 147–154.

[32] X. Kanga, J. Wanga, H. Wua, J. Liua, I. A. Aksayc, Y. Lin, A graphene-based electrochemical sensor for sensitive detection of paracetamol, Talanta, 2010, 81, 754–759.

[33] Y. Fan, J.-H. Liu, H.-T. Lu, Q. Zhang, Electrochemical behavior and voltammetric determination of paracetamol on Nafion/TiO_2–graphene modified glassy carbon electrode, Colloids and Surfaces B: Biointerfaces, 2011, 85, 289–292.

[34] R. N. Goyal, S. P. Singh, Voltammetric determination of paracetamol at C_{60}-modified glassy carbon electrode, Electrochimica Acta, 2006, 51, 3008–3012.

[35] M. Li, L. Jing, Electrochemical behavior of acetaminophen and its detection on the PANI–MWCNTs composite modified electrode, Electrochimica Acta, 2007, 52, 3250–3257.

[36] F. S Felix, C. M Brett, L. Angnes, Carbon film resistor electrode for amperometric determination of acetaminophen in pharmaceutical formulations, J. Pharm. Biomed. Anal. 2007, 43, 1622-1627.

[37] N. Nasirizadeh, H. R Zare, Differential pulse voltammetric simultaneous determination of noradrenalin and acetaminophen using a hematoxylin biosensor, Talanta, 2009, 80, 656-663.

[38] E. de S. Gil, G. R. de Melo, Electrochemical biosensors in pharmaceutical analysis, Braz. J. Pharm. Sc. 2010, 46, no. 3.

[39] R. T. Kachoosangi, G. G. Wildgoose, R. G. Compton, ComptonSensitive adsorptive stripping voltammetric determination of paracetamol at multiwalled carbon nanotube modified basal plane pyrolytic graphite electrode. Analytica Chimica Acta, 2008, 618, 54–60.

[40] N. Wangfuengkanagul, O. Chailapakul, Electrochemical analysis of acetaminophen using a boron-doped diamond thin film electrode applied to flow injection system, J. Pharm. Biomed. Anal. 2002, 28, 841–847.

[41] H.-L. Jiang, B. Liu, Y.-Q. Lan, K. Kuratani, T. Akita, H. Shioyama, F. Zong, Q. Xu, From Metal–Organic Framework to Nanoporous Carbon: Toward a Very High Surface Area and Hydrogen Uptake, J. Am. Chem. Soc. 2011,133, 11854–11857.

[42] H. Wang, Q. Gao, J. Hu, High Hydrogen Storage Capacity of Porous Carbons Prepared by Using Activated Carbon J. Am. Chem. Soc. 2009, 131,7016–7022.

[43] B. Liu, H. Shioyama, T. Akita, Q. Xu, Metal-Organic Framework as a Template for Porous Carbon Synthesis, J. Am. Chem. Soc. 2008, 130, 5390–5391.

[44] Q. Li, J. Yang, D. Feng, Z. Wu, Q. Wu, S. S. Park, C.-S. Ha, D. Zhao, Facile Synthesis of Porous Carbon Nitride Spheres with Hierarchical Three-Dimensional Mesostructures for CO_2 Capture, Nano Res. 2010, 3, 632–642.

[45] B. Friedel, S. Greulich-Weber, Preparation of Monodisperse Submicrometer Carbon Spheres by Pyrolysis of Melamine–Formaldehyde Resin, Small, 2006, 2, 859–863.

[46] C. Gao, S. Moya, H. Lichtenfeld, A. Casoli, H. Fiedler, E. Donath, H. Möhwald,The Decomposition Process of Melamine Formaldehyde Cores: The Key Step in the Fabrication of Ultrathin Polyelectrolyte Multilayer Capsules, Macromol. Mater. Eng. 2001, 286, 355-361.

[47] R. S. Nicholson, Theory and Application of Cyclic Voltammetry for Measurement of Electrode Reaction Kinetics, Anal. Chem. 1965, 37, 1351–1355.

[48] X. Kang, J. Wang, H. Wu, J. Liu, I.A. Aksay, Y. Lin, A graphene-based electrochemical sensor for sensitive detection of paracetamol, Talanta, 2010, 81, 754-759.

[49] K.-C. Lin, Y.-S. Li, S.-M. Chen, Electrochemical Determination of Ascorbic Acid Using Poly(Xanthurenic Acid) and Multi-Walled Carbon Nanotubes, Int. J. Electrochem. Sci. 2012, 7, 12752 – 12763.

[50] C. Wang, R. Yuan, Y. Chai, S. Chen, F. Hu, M. Zhang, Simultaneous determination of ascorbic acid, dopamine, uric acid and tryptophan on gold nanoparticles/overoxidized-polyimidazole composite modified glassy carbon electrode, Anal. Chim. Acta, 2012, 41, 15-20.

[51] G. Scandurra, A. Antonella, C. Ciofi, G. Saitta, M. Lanza , Electrochemical Detection of *p*-Aminophenol by Flexible Devices Based on Multi-Wall Carbon Nanotubes Dispersed in Electrochemically Modified Nafion, Sensors, 2014, 14, 8926-8939.

[52] H. Yin, Q. Ma, Y. Zhou, S. Ai, L. Zhu, Electrochemical behavior and voltammetric determination of 4-aminophenol based on graphene–chitosan composite film modified glassy carbon electrode, Electrochimica Acta, 2010, 55, 7102–7108.

[53] H. Yin, Q. Ma, Y. Zhou, S. Ai, L. Zhu, Electrochemical behavior and voltammetric determination of 4-aminophenol based on graphene–chitosan composite film modified glassy carbon electrode, Electrochimica Acta, 2010, 55, 7102–7108.

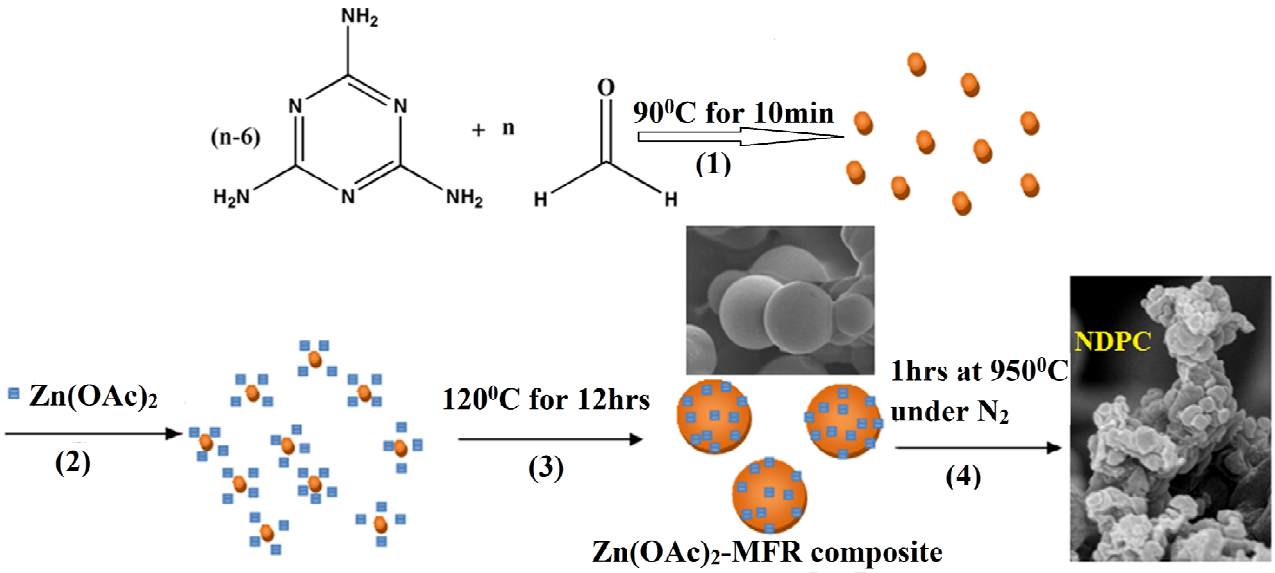

Scheme 1. Illustration of formation of NDPC, in (1st step) formation of soluble melamine-formaldehyde resin, (2nd step) formation of $Zn(OAc)_2$-MFR composites, (3rd step) cross-linking between MFR progresses and in (4th step) removal of Zn species with formation of the NDPC.

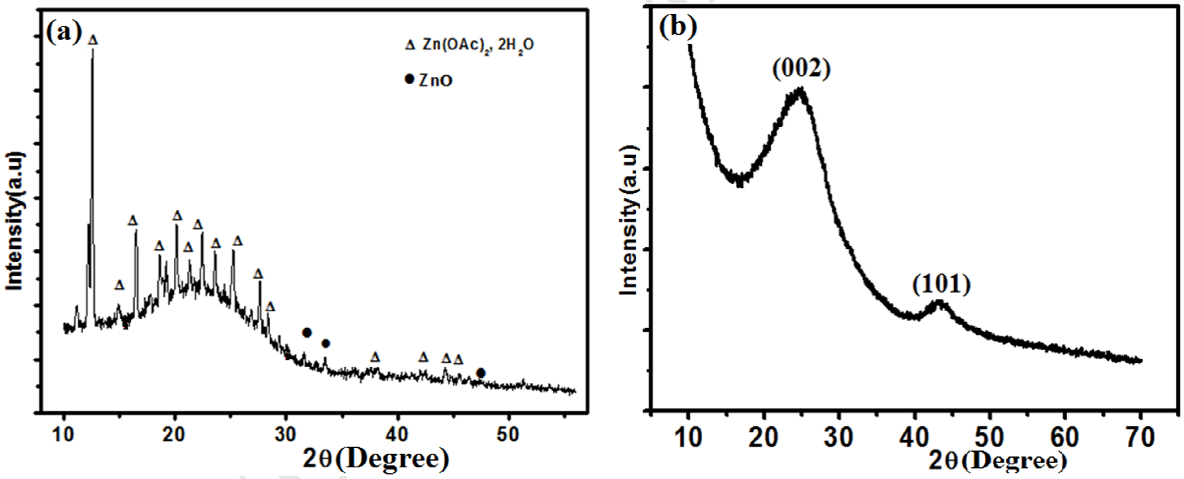

Figure 1. X-ray diffraction(XRD) of (a) ZAIMFR and (b) NDPC

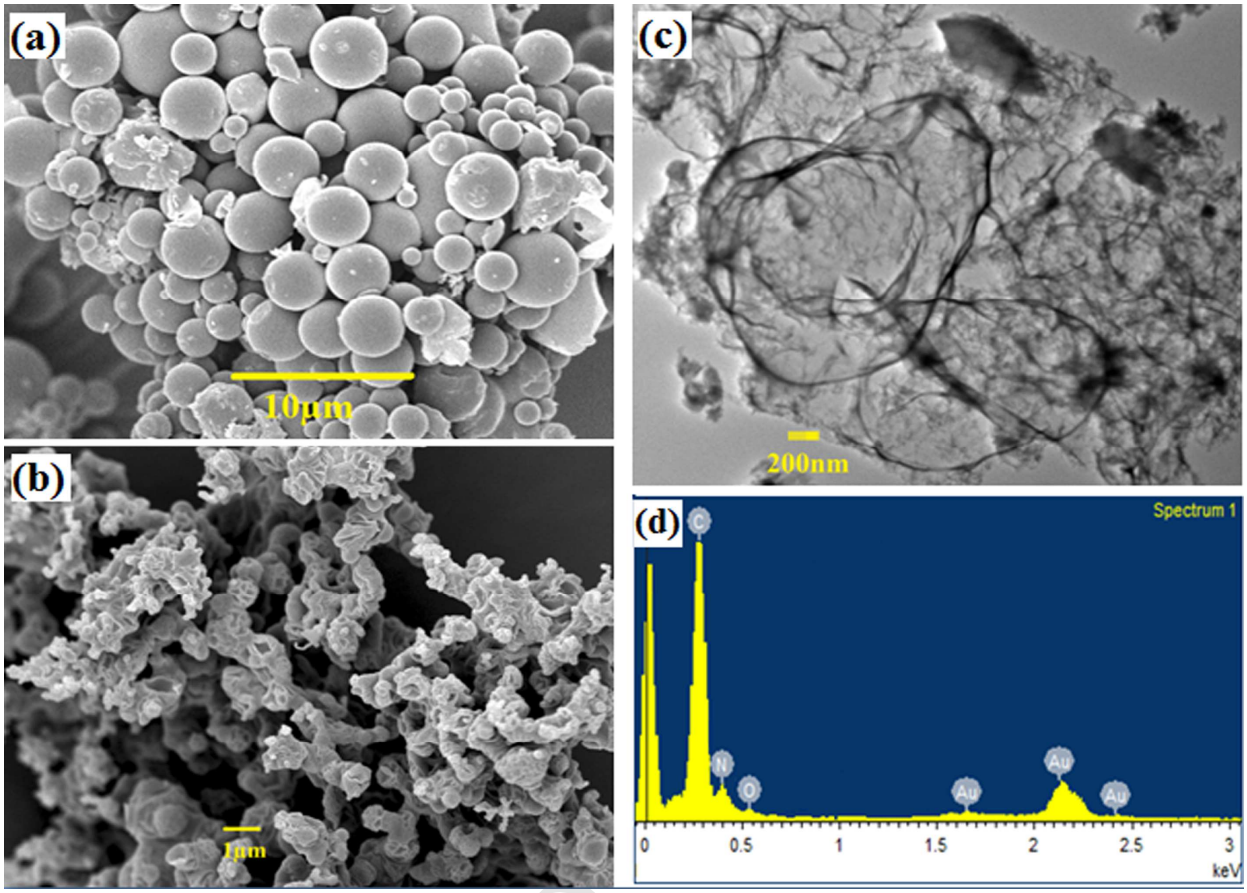

Figure 2. (a) FESEM image of ZAIMFR, (b) and (c) FESEM and TEM image of NDPC, (d) EDS spectra of NDPC.

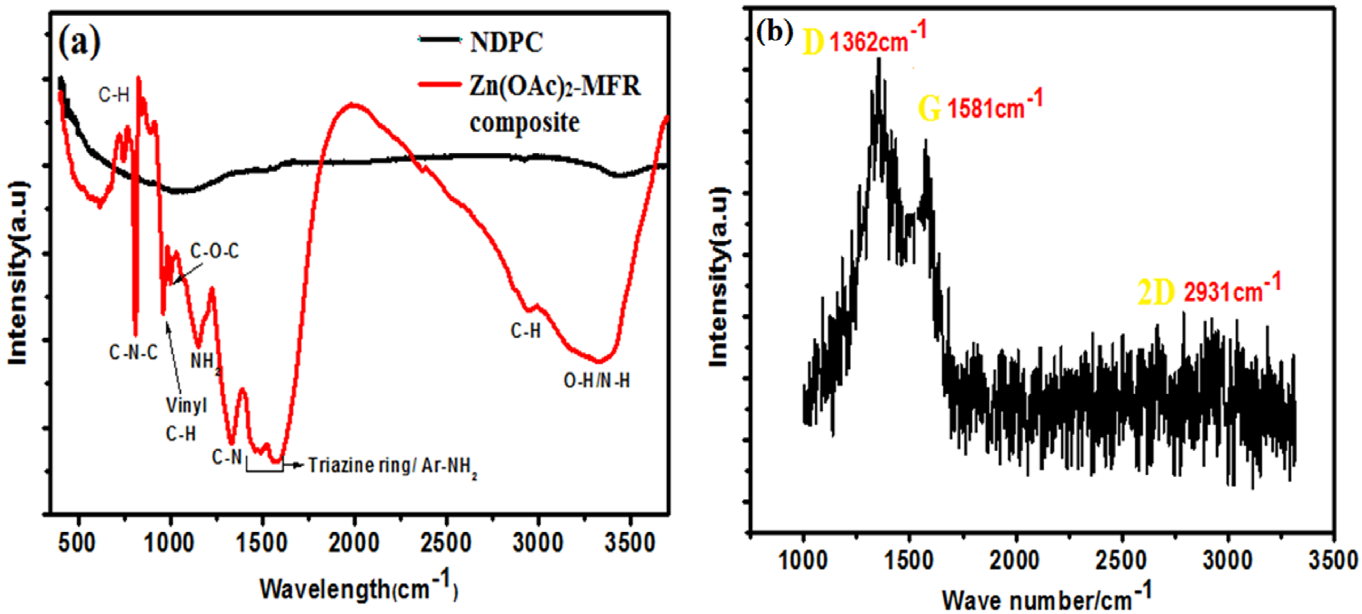

Figure 3. (a) FTIR spectra of ZAIMFR microsphere (red) and NDPC (black). (b) Raman spectra of NDPC.

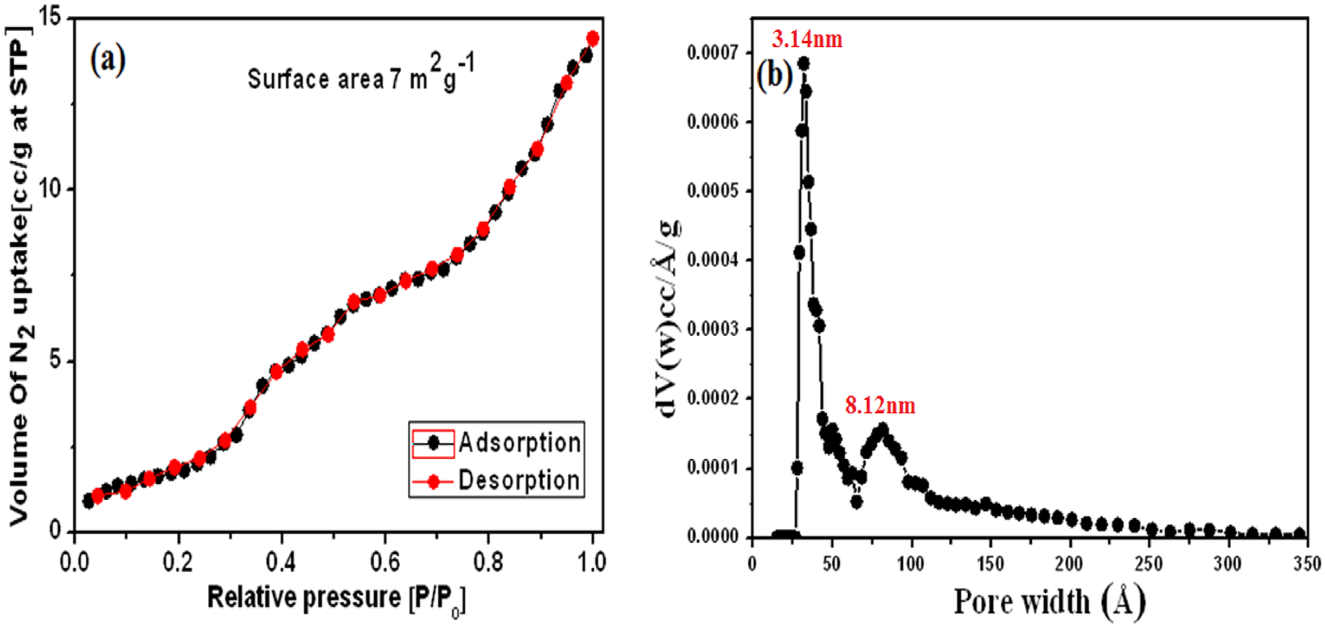

Figure 4. (a) Nitrogen adsorption–desorption isotherms (black and red symbols represent adsorption and desorption isotherms, respectively) and (b) corresponding BJH pore size distributions of the NDPC.

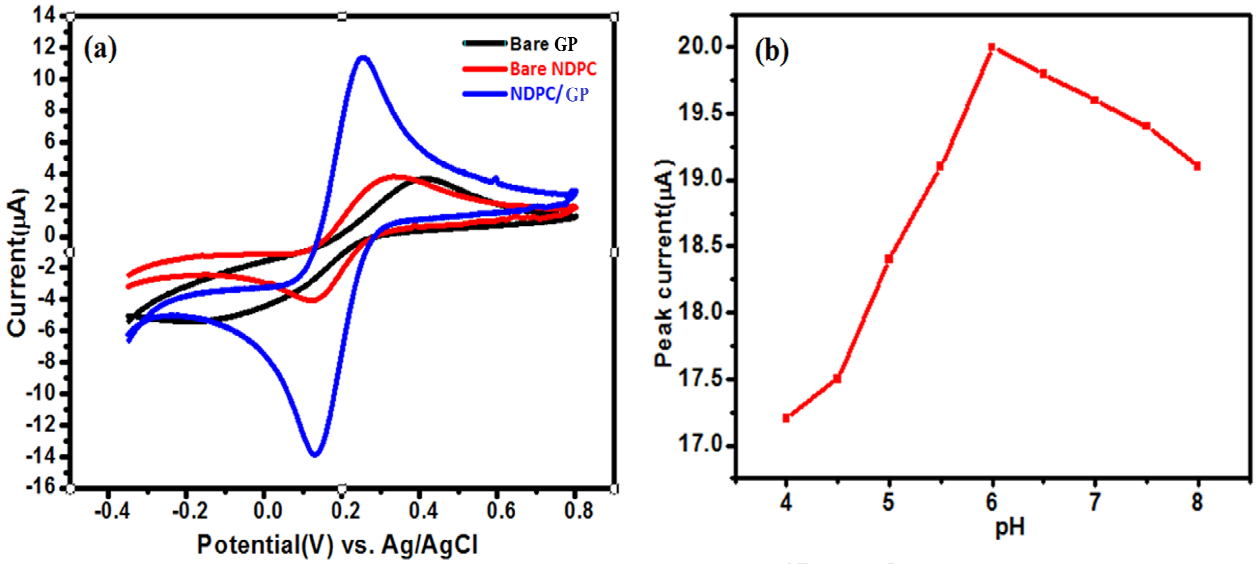

Figure 5. (a) CVs obtained for 1mM $Fe(CN)_6^{-4}/Fe(CN)_6^{-3}$ at NDPC/GP (blue), bare GP (black) and bare NDPC(red) electrode (b) pH *vs.* peak current (I_{PCM}) of 0.5 mM PCM at NDPC/GC electrode. Scan rate for CVs: $100mVs^{-1}$.

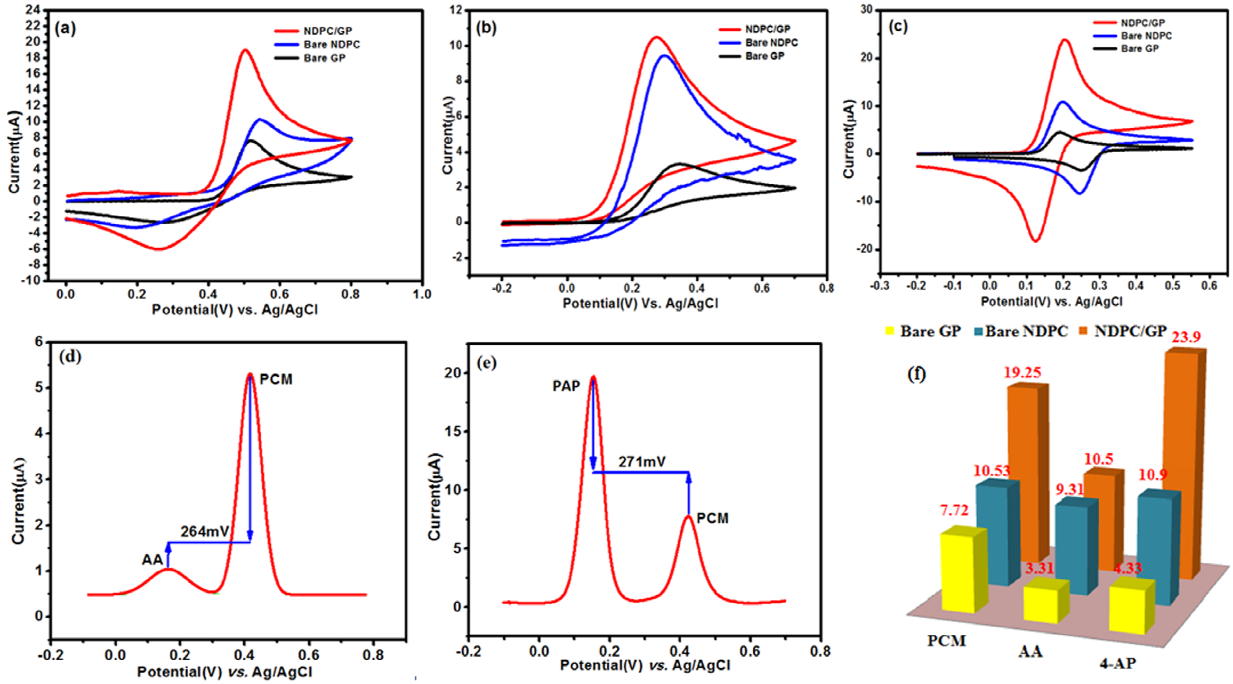

Figure 6. CVs of at bare GP (black), bare NDPC (blue) and NDPC/GP (red) electrodes of (a) 0.5mM PCM; (b) 0.5mM AA and (c) 0.5mM PAP in 0.1(M) phosphate buffer pH 6.0; DPV of (d) 0.1mM of PCM + 0.1mM of AA mixture and (e) 0.1mM of PCM + 0.1mM of PAP mixture at NDPC/GP electrode in 0.1(M) phosphate buffer pH 6.0. (f) Comparison of electrocatalytic activity of all electrodes for each individual molecule. Scan rate for CVs: 100mVs^{-1} and for DPVs: 50mVs^{-1}.

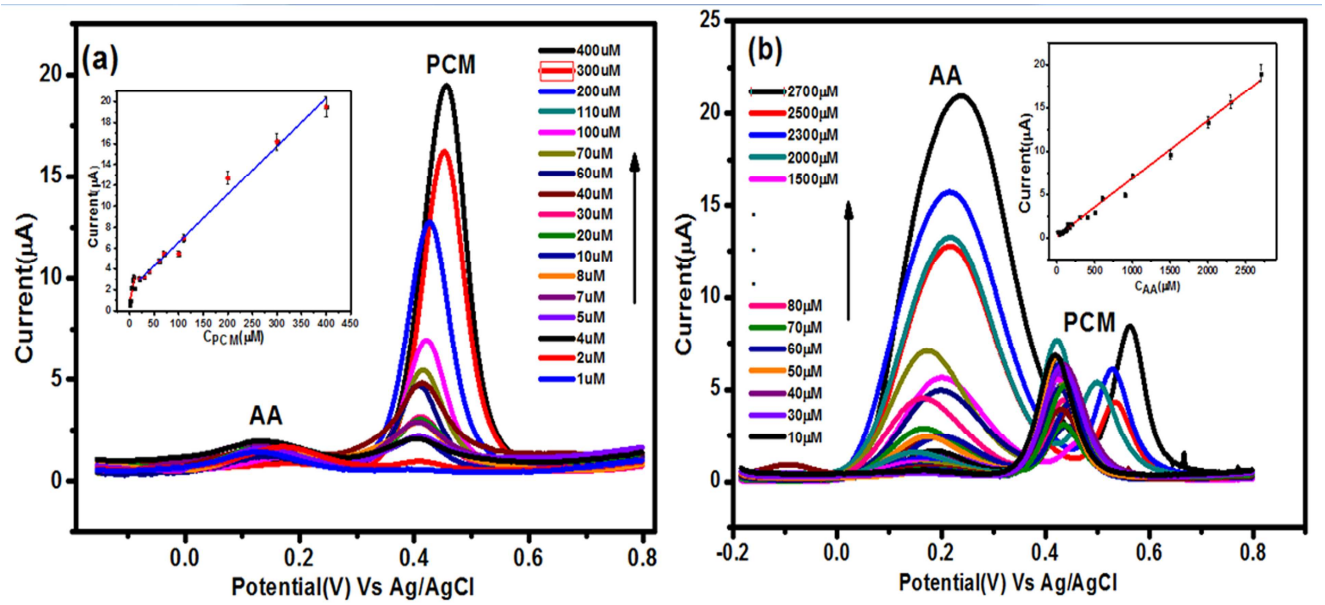

Figure 7. DPVs at NDPC/GP electrode in 0.1(M) PBS (pH 6.0) (a) containing 10 mM AA and different concentrations of PCM: 1, 2, 4, 5, 7, 8, 10, 20, 30, 40, 50, 60, 70, 80, 90, 100, 110, 200, 300, 400 μM; Inset Corresponding peak current(I_{PCM}) vs. concentration(C_{PCM}) curve; (b) containing 0.1 mM PCM and different concentrations of AA: 10, 30, 40, 50, 60, 70, 80, 90, 110, 120, 130, 140, 150, 160, 170, 180, 190, 200, 300, 400, 500, 600, 900, 1000, 1500, 2000, 2300, 2700 μM; Inset Corresponding concentration(C_{AA}) vs. peak current(I_{AA}) curve;

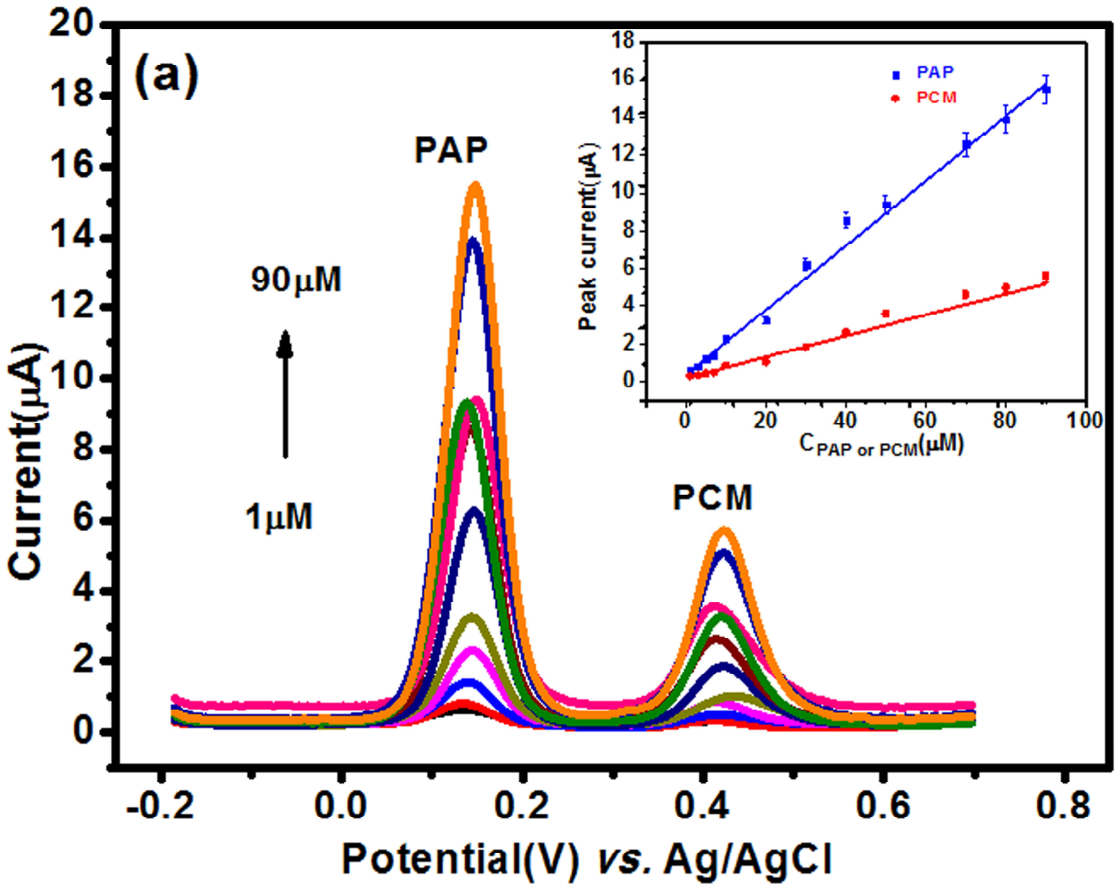

Figure 8. (a) DPVs of 1, 3, 5, 7, 10, 20, 30, 40, 50, 60, 80 and 90 µM of PAP and PCM at NDPC/GP electrode in 0.1 (M) phosphate buffer pH 6.0; Inset Corresponding peak current($I_{PCM\ or\ PAP}$) *vs.* concentration($C_{PCM\ or\ PAP}$).

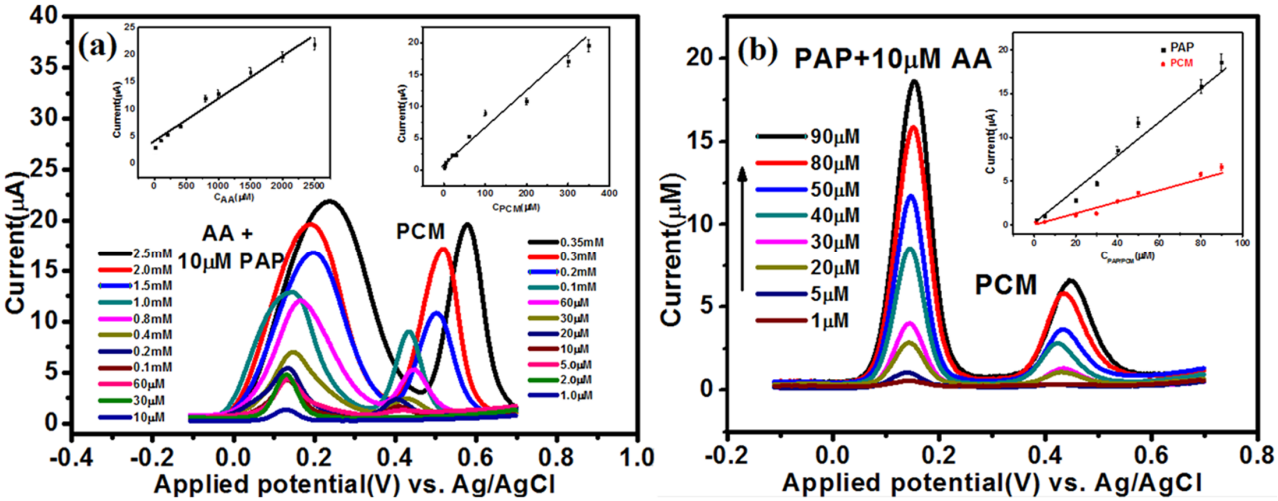

Figure 9. DPVs at NDPC/GP electrode in 0.1(M) PBS (pH 6.0) (a) containing 10μM PAP and different concentrations of PCM and AA: (1+10), (2+30), (5+60), (10+100), (20+200), (30+400), (60+800), (100+1000), (200+1500), (300+2000), (350+2500) μM; Inset Corresponding peak current($I_{PCM/AA}$) vs. concentration($C_{PCM/AA}$) curve; (b) DPVs of 1, 5, 20, 30, 40, 50, 80 and 90 μM of PAP and PCM at NDPC/GP electrode in 0.1 (M) phosphate buffer of pH 6.0; Inset Corresponding peak current($I_{PCM\ or\ PAP}$) *vs.* concentration($C_{PCM\ or\ PAP}$).

Table 1. A comparison with other reported literatures

Electrode	Linear range(μM)			Detection limit(μM)			Ref.
	PCM	AA	PAP	PCM	AA	PAP	
Graphene/GCE	0-20	-	-	0.032	-	-	[32]
Nafion/TiO_2–graphene/GCE	1-100	-	-	0.21	-	-	[33]
C_{60}/GCE	50-1500	-	-	-	-	-	[34]
PANI-MWCNT/GCE	1-100, 250-2000	-	-	0.25	-	-	[35]
SWCNT/PGE[a]	0.2-100	-	-	0.12	-	-	[39]
Poly(Xanthurenic Acid)/MWCNT	-	1-1520	-	-	0.1	-	[49]
GNPs/PImox[b]	-	210-1010	-	-	2.0	-	[50]
SWCNT/GCE	-	-	0.2-1.6	-	-	0.090	[51]
Graphen-PANI/GCE	10-100	-	0.2-20-100	-	-	0.065	[52]
Graphene–chitosan/GCE	-	-	0.2-550	-	-	0.057	[53]
NDPC/GP	**1-7, 8-400**	**10-2700**	**-**	**0.030**	**0.72**	**0.010**	**This**
	1-90	**-**	**1-90**				**work**

[a] Single wall Carbon nanotube/ pyrolytic graphite electrode

[b]Gold nanoparticles decorated overoxidized-polyimidazol film

1. Synthesis of porous nitrogen doped carbon using Zinc acetate as hard template from easily available precursors.
2. Nitrogen doped carbon shows superior electrocatalytic properties.
3. Analysis of Paracetamol in biological and pharmaceuticals sample.

Supplementary Information

Electrochemical Determination of Paracetamol in Presence of Ascorbic acid and *p*-Aminophenol using Nitrogen doped Porous Graphitic Carbon.

Sudip Biswas[1], Dipanjan Chakraborty[1], Rashmita Das[1], Rajib Bandyopadhyay[1], Panchanan Pramanik[2*]

[1]Department of Instrumentation and Electronics Engineering, Jadavpur Universiy Salt lake Campus, Kolkata-700098.

[2] Department of Basic Science, MCKV Institute of Engineering, Liluah, West Bengal-711204

E-mail: pramanik1946@gmail.com

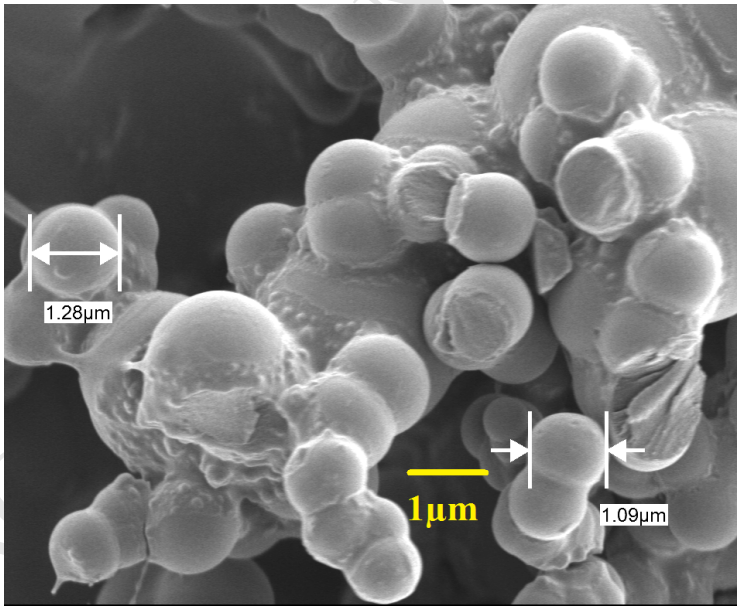

Figure S1. FESEM of ZAIMFR

Table S3. Analysis of PCM in pharmaceutical samples (n=3):

	Content(µM)	Spiking(µM) PCM	PAP	AA	Found(µM)	R.D.S[d](%)	Recovery[e](%)
PCM in Injection	10.46[c]	10	20	50	20.60	1.3	100.7
PCM Tablet	50.57[c]	10	20	50	60.78	1.6	100.3

[c]Average of three measurement(R.S.D=2.3)

[d]Relative standard deviation

[e]Recovery=$\frac{\text{Found}(\mu M)-\text{Diluted urine/pharmaceutical sample}(\mu M)}{\text{Spiking}(\mu M)}$

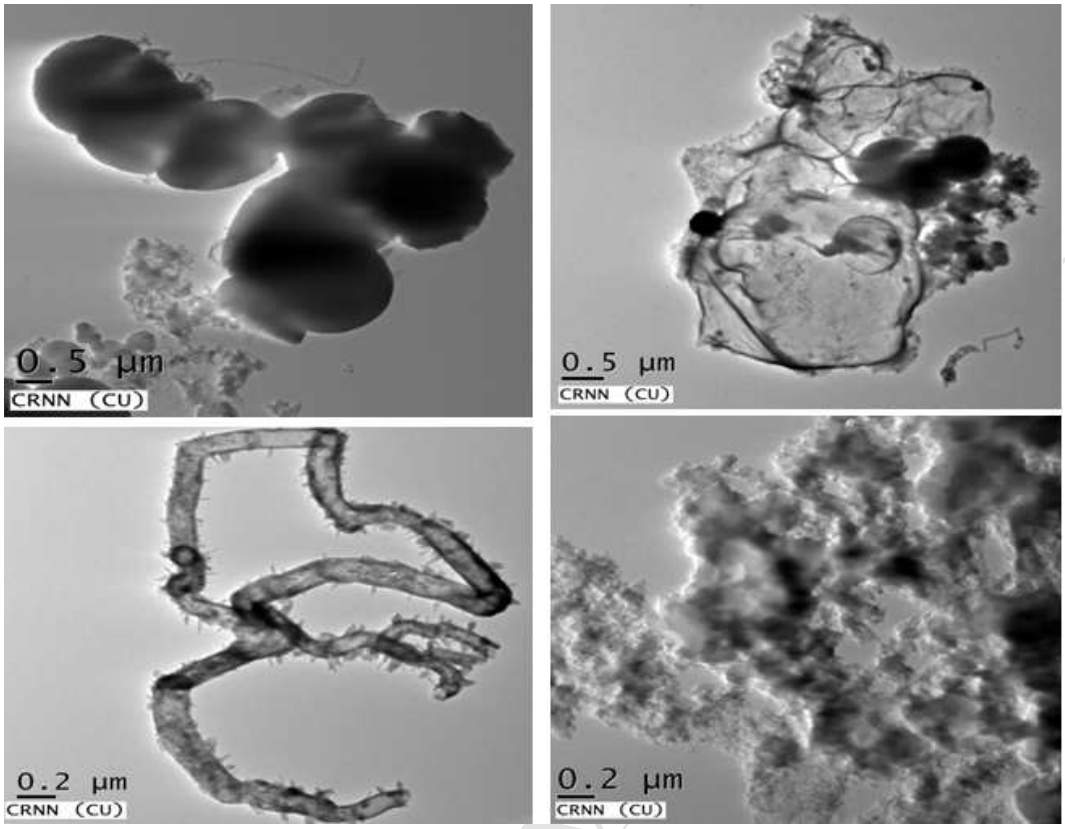

Figure S2. TEM images of NDPC

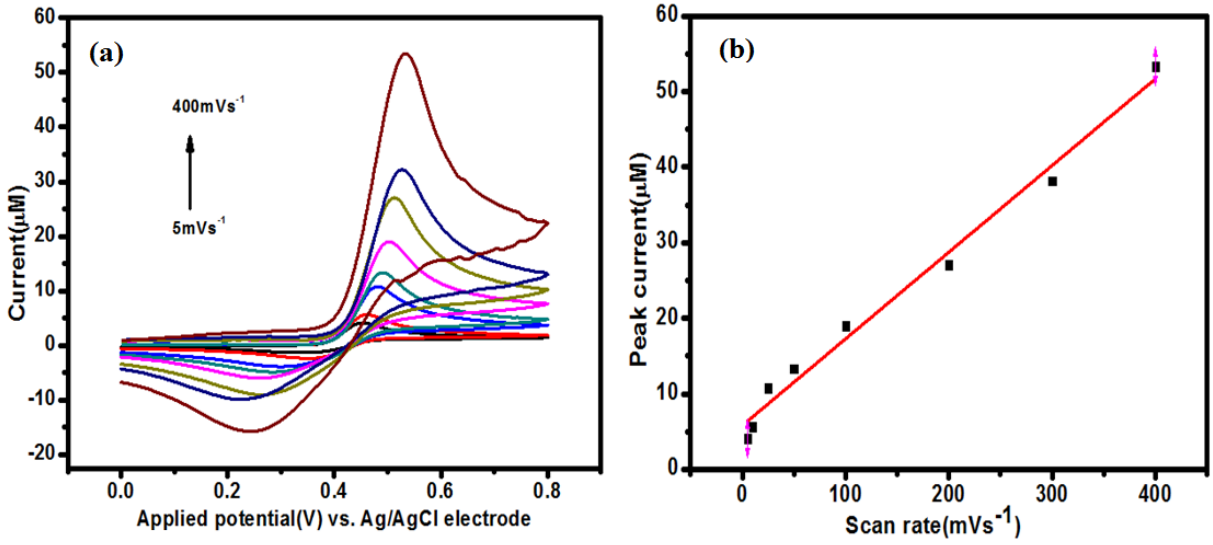

Figure S3. (a) CVs of 0.5mM PCM at NDPC/GP with scan rate ranging from 5mVs^{-1} to 400mVs^{-1} at pH 6. And (b) Corresponding oxidation peak current (I_{PCM}) vs. scan rate curve (mVs^{-1})

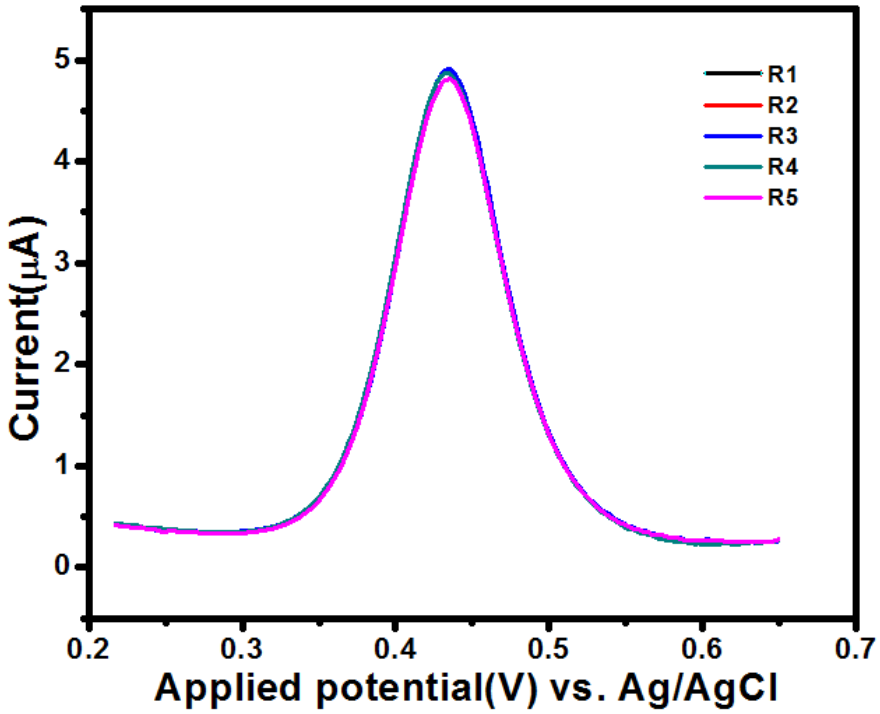

Figure S4. Five successive DPV measurements of 0.1mM PCM in presence of 0.1mM AA and PAP

Table S1. EDS analysis of NDPC

Sample	N in atomic %	C in atomic %	O in atomic %
NDPC	12.6	82.20	5.20

Table S2. Determination of PCM, AA, and PAP in urine sample using NDPC/GP (n=3):

	Diluted urine sample(μM)	Spiking(μM) PCM	AA	PAP	Found(μM)	R.S.D[d](%)	Recovery[e](%)
PCM	12.65[c]	10	50	20	23.2	1.4	102.0
AA	0	10	50	0	49.96	2.1	99.9
PAP	0	10	0	20	20.24	1.2	101.2